Optical evidence for a Weyl semimetal state in pyrochlore Eu₂Ir₂O₇

A. B. Sushkov,[1,*] J. B. Hofmann,[2] G. S. Jenkins,[1] J. Ishikawa,[3] S. Nakatsuji,[3,4] S. Das Sarma,[2] and H. D. Drew[1]

[1]*Center for Nanophysics and Advanced Materials, Department of Physics, University of Maryland, College Park, Maryland 20742, USA*

[2]*Condensed Matter Theory Center and Joint Quantum Institute, Department of Physics, University of Maryland,*
College Park, Maryland 20742, USA

[3]*Institute for Solid State Physics, University of Tokyo, Kashiwa, Chiba 277-8581, Japan*

[4]*PRESTO, Japan Science and Technology Agency (JST), 4-1-8 Honcho Kawaguchi, Saitama 332-0012, Japan*

A Weyl semimetallic state with pairs of nondegenerate Dirac cones in three dimensions was recently predicted to occur in the antiferromagnetic state of the pyrochlore iridates. Here, we show that the THz optical conductivity and temperature dependence of the free carrier response in pyrochlore Eu₂Ir₂O₇ match the predictions for a Weyl semimetal and suggest novel Dirac liquid behavior. The interband optical conductivity vanishes continuously at low frequencies signifying a semimetal. The metal-semimetal transition at $T_N = 110$ K is manifested in the Drude spectral weight, which is independent of temperature in the metallic phase and decreases smoothly in the ordered phase. The temperature dependence of the free carrier weight below T_N is in good agreement with theoretical predictions for a Dirac material. The data yield a Fermi velocity $v_F \approx 4 \times 10^7$ cm/s, a logarithmic renormalization scale $\Lambda_L \approx 600$ K, and require a Fermi temperature of $T_F \approx 100$ K associated with residual unintentional doping to account for the low temperature optical response and dc resistivity.

Condensed matter physics is in an exciting new era dominated by Dirac materials and topological effects. The introduction of topology, particularly in association with spin-orbit coupling, has led to predictions of novel electronic and optical phenomena [1–4]. The most recent development is the discovery of three-dimensional (3D) Dirac [5–10] and Weyl [11–13] materials, where the Dirac cones come in pairs and have non-Kramers degenerate chiral bands protected by topology. A 3D Weyl state has been predicted [14] for the $5d$ transition metal oxide family of pyrochlore iridates [15], which are strongly interacting materials with a strong spin-orbit interaction. However, in the absence of direct experimental evidence, their ground state is still under intense discussion [16–19].

The pyrochlore iridates $R_2\text{Ir}_2\text{O}_7$ are strongly interacting materials that exhibit frustrated magnetism and an associated metal-insulator transition as R varies across the rare earth series [20]. Due to a strong spin-orbit interaction these materials have been recognized as having potentially exotic ground states including the Weyl semimetallic state in the low temperature magnetic phase. Also, axion insulator [14,16], topological band insulator and Mott insulator [1], and spin liquid states [21,22] have been proposed. X-ray diffraction experiments show that there is no structural transition breaking the cubic symmetry in Nd, Eu, and Pr pyrochlores, and that the Eu compound displays a smooth thermal contraction of the lattice parameters through the "metal-insulator" transition [23]. Ueda *et al.* [24] reported a 50 meV optical gap in the ground state of polycrystalline Nd₂Ir₂O₇ which was tuned to zero by the partial substitution of Ir by Rh, and that gapless state was proposed to be a Weyl semimetal. By contrast, infrared studies of Bi₂Ir₂O₇ found a strongly metallic ground state [25]. Therefore, at present there is no clear evidence of the predicted Weyl semimetal state in the rare earth pyrochlores.

Here, we present evidence of a Weyl semimetal on the basis of experimental and theoretical studies of the optical response,

and we identify the electronic phase transition in Eu₂Ir₂O₇ at T_N as a metal-semimetal transition in which the conductance is controlled by the thermal population of the Weyl cones. Single crystals of Eu₂Ir₂O₇ were grown as described elsewhere [26]. Our crystal has the same dc conductivity as the sample #2 of Ref. [26]. Fourier transform infrared reflectivity and transmission measurements were performed on the 1.8 mm in diameter (111) face of a single crystal. For transmission measurements at frequencies below 100 cm⁻¹, the crystal was glued down to an intrinsic Si substrate using transparent Stycast epoxy and was polished down to ≈10 micron.

Figure 1 shows the measured reflectivity and transmission spectra of Eu₂Ir₂O₇ over a broad frequency range. The transmission measured at 7 K immediately suggests a semimetallic state. The negative slope implies an optical conductivity growing with frequency. An insulator (or gapped state) would give a flat transmission, and a free carrier Drude term would give a slope of opposite sign.

We have analyzed the reflectivity and transmission spectra in two standard ways [27]: first, using a model of a sum of Lorentzian oscillators and second, using a variational dielectric function (equivalent to a Kramers-Kronig transformation) [28]. In the first method, we fit the reflectivity and the transmission spectra of Eu₂Ir₂O₇ using a Lorentzian model, in which the complex dielectric function $\varepsilon = \varepsilon_1 + i\varepsilon_2$ takes the form:

$$\varepsilon(\omega) = \varepsilon_\infty + \sum_j \frac{\omega_{sj}^2}{\omega_{0j}^2 - \omega^2 - i\omega\gamma_j}. \tag{1}$$

Here ω_{0j}, γ_j, and ω_{sj} are the resonance, the damping, and the spectral weight frequencies of the jth electric dipole active mode, respectively. For the present system, we use a Drude term, seven symmetry allowed phonons [29], and we find that the electronic response can be well represented using five electronic transitions, the lowest one at $\omega_0 = 306$ cm⁻¹ with $\gamma = 1143$ cm⁻¹. In the second method, we use the results of the first method as a starting spectrum for the variational $\varepsilon(\omega)$ to account for small deviations [27]. The complex
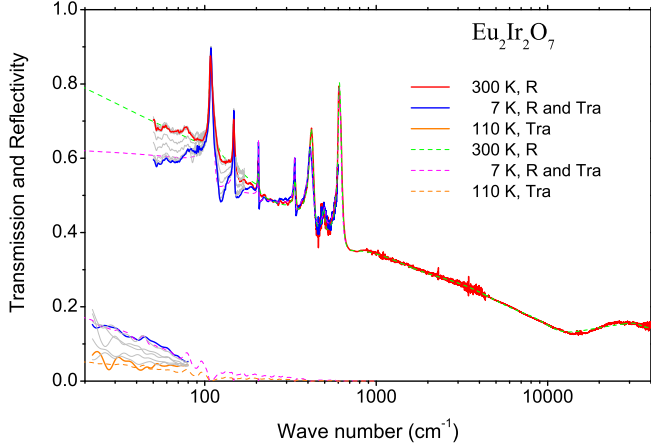
————
*Corresponding author: sushkov@umd.edu

FIG. 1. (Color online) Reflectivity (R) and transmission (Tra) of a $Eu_2Ir_2O_7$ single crystal. Dashed curves are fits using the Lorentzian model [Eq. (1)]. Gray lines are spectra at intermediate temperatures. The temperature dependence was measured over a 20–6000 cm^{-1} frequency range.

FIG. 2. (Color online) Optical conductivity and dielectric constant of a $Eu_2Ir_2O_7$ single crystal. (a) Temperature-independent broad band electronic optical conductivity. (b) Temperature-dependent low-frequency part of the optical conductivity. Our zero frequency values are close to the dc measurements [26]. The magenta line is a linear fit of equation (2) to the conductivity. (c) The dielectric constant. The continuous green line is the blue 7 K line with the phonon contributions removed. The dashed black line denotes the high-frequency dielectric constant κ obtained from the plasmon fit.

optical conductivity is related to the dielectric function by $\sigma = \sigma_1 + i\sigma_2 = \omega\varepsilon/4\pi i$.

Figure 2 presents the frequency-dependent optical conductivity σ_1 and the dielectric constant ε_1 as obtained from the analysis of the experimental spectra. Figure 2(a) shows the optical conductivity in a broad frequency range as obtained from the variational ε analysis. The two-peak conductivity spectra are consistent with resonant inelastic x-ray scattering spectra [30] and band structure calculations [16]. The vanishing of σ_1 at low frequencies is a signature of a Dirac semimetal. The 1 eV band consists of transitions within the $J_{eff} = 1/2$ bands [16]. Figures 2(b) and 2(c) show the optical conductivity and the dielectric constant at low frequencies. The increasing ε_1 at low frequencies [Fig. 2(c)] is another characteristic of a semimetal and is expected to diverge logarithmically for an intrinsic Weyl semimetal in the absence of disorder [31]. The optical conductivity of an intrinsic Weyl semimetal can be written as

$$\sigma_1 = \frac{g}{12} \times \frac{e^2}{h} \times \frac{\omega}{\bar{v}_F}, \qquad (2)$$

arising from interband excitations within the Dirac cone [14]. Here, we denote by g the degeneracy of Dirac nodes and by $\bar{v}_F = (v_F^x v_F^y v_F^z)^{1/3}$ the geometric mean of the Fermi velocities. By fitting this expression to the optical conductivity [magenta line in Fig. 2(b)] using $g = 24$ [14], we obtain $\bar{v}_F = 3.4 \times 10^7$ cm/s.

Based on this fit to the optical conductivity, we can extract the Coulomb interaction strength in the semimetal as given by the effective Dirac fine structure constant $\alpha = e^2/\hbar v_F \kappa$. Here, κ, which is of the order of 10, is the high-frequency dielectric constant which shows no temperature dependence as is evident in Fig. 2(c). [We use ϵ and κ to designate experimental and theoretical dielectric constant, respectively.] This gives a bare value of $\alpha = 0.7$ for the interaction strength, indicating that electron interaction could have considerable impact on the low-energy properties of this Dirac material. Since the corresponding fine structure constant for quantum electrodynamics is 1/137, the current problem is a
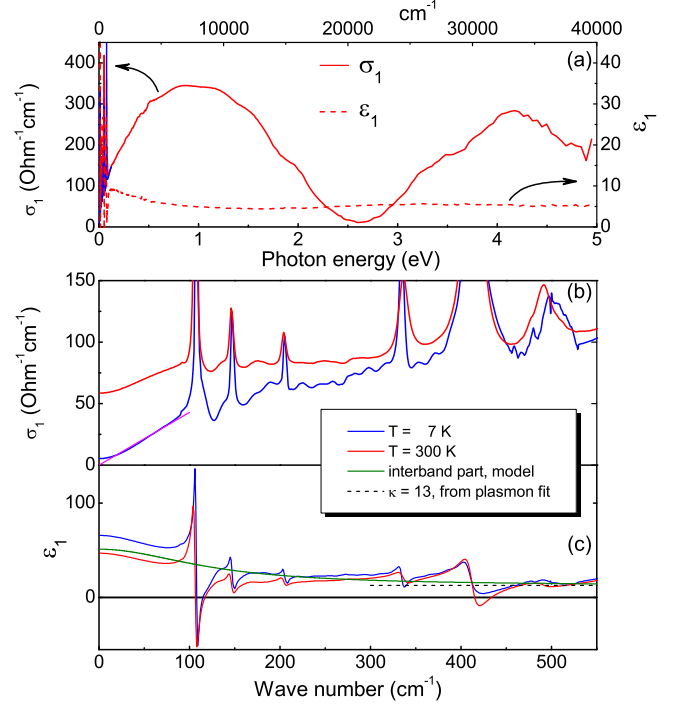
strong-coupling (and nonrelativistic) version of quantum electrodynamics.

The conductivity exhibits a temperature dependence only at low frequencies $\omega < 500$ cm^{-1}. Fits of Eq. (1) to the experimental spectra reveal that only the Drude and phonon terms are temperature dependent while the interband conductivity can be kept constant at all temperatures. The validity of this conclusion is verified by a spectral weight analysis presented in the Supplemental Material [27]. We show the result for the experimental Drude spectral weight and scattering γ as a function of temperature in Figs. 3(a) and 3(b). The metal-semimetal transition at T_N is manifested as a smooth decrease of the Drude spectral weight in the Weyl state which can exist only below T_N where time-reversal symmetry is broken [14].

In Fig. 3(a), we compare the experimental Drude weight with the theoretical prediction for a Dirac liquid. The low-temperature saturation indicates a finite Fermi energy E_F (associated with unintentional residual doping), leads to a low temperature dc conductivity, and marks a transition between an extrinsic metallic low-temperature regime ($k_B T < E_F$) and an intrinsic semimetallic high-temperature regime ($k_B T > E_F$). Our observations are consistent with the Drude weight as predicted by kinetic theory,

$$\omega_{sD}^2 = -\frac{e^2 \bar{v}_F^2}{3} \int_{-\infty}^{\infty} dE\, D(E)\, \frac{\partial f(E)}{\partial E}, \qquad (3)$$
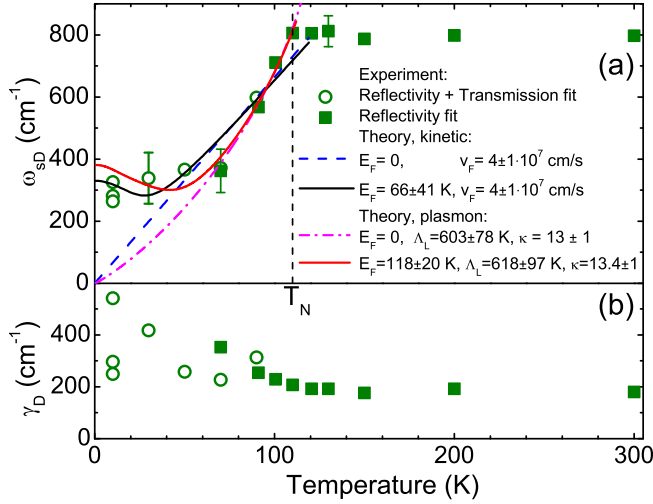
FIG. 3. (Color online) Temperature dependence of the spectral Drude weight and scattering rate γ. (a) Open circles—results of simultaneous fit of reflectivity and transmission, solid squares—results of reflectivity fits, both using Eq. (1), lines—fits of kinetic theory [Eq. (3)] and plasmon to these experimental points below T_N. (b) Experimental scattering rate of free carriers.

where $D(E) = gE^2/[2\pi^2(\hbar\bar{v}_F)^3]$ is the density of states and $f(\varepsilon)$ the Fermi-Dirac distribution. A fit of the Drude weight [solid black line in Fig. 3(a)] gives a finite Fermi energy of $E_F/k_B \approx 70$ K and a Fermi velocity of $\bar{v}_F = 4 \times 10^7$ cm/s, in agreement with the direct fit to the frequency-dependent conductivity. For comparison, we include a fit to the high-temperature Drude weight in the strictly intrinsic limit [dashed blue line in Fig. 3(a)] which shows that finite doping does not affect the Drude weight at high temperature ($k_B T > E_F$). Note that for a general semimetallic dispersion $E \sim |k|^z$, the Drude weight is expected to scale as $\omega_{sD}^2 \sim T^{1+1/z}$ with temperature [32]. The superlinear temperature dependence implies $z < 1$ in this effective model, compellingly excluding, for example, a parabolic semimetallic ground state.

Our experimental Drude weight is seen to deviate from the strict linear temperature scaling of a noninteracting semimetal, which can be attributed to electron interactions: The interaction strength of an intrinsic Dirac semimetal acquires a scale dependence due to ultraviolet renormalization, giving rise to a superlinear temperature dependence of the Drude weight and providing a direct signature of electron interaction effects [31,33]. Within RPA, the temperature dependence of the interaction strength is given by [33,34]

$$\alpha(T) = \frac{3\pi}{g} \ln^{-1} \frac{\Lambda_L}{T}. \qquad (4)$$

Instead of depending on e^2, $\bar{v}_F$, and κ separately, this expression contains a single renormalized energy scale Λ_L, the Landau pole, at which the coupling α diverges. This Landau scale is an effective parameter of the system that can be extracted from measurements of the Drude weight and corresponds to a cutoff scale beyond which the Dirac dispersion is no longer linear. In the present system, it can be

associated with the Lifshitz saddle point between each pair of Weyl points [33].

In the absence of disorder and phonon contributions, the Drude weight corresponds to the plasmon frequency as defined by the zero of the dielectric function $\varepsilon(\omega) = \kappa_0 - \omega_{sD}^2/\omega^2$. We assume κ_0 independent of T and ω [Fig. 2(c)], and it is a good assumption in the frequency range 300–800 cm^{-1} where solutions for ω_{sD} are found. We perform a fit to the experimental ω_{sD} using the plasmon dispersion of an extrinsic Dirac semimetal [33], which fully takes into account the competing effects of finite doping and renormalization of the interaction. Since theoretical calculations only predict the renormalization of the effective fine structure constant α, there is a question whether renormalization effects should be manifested in the Drude weight, the dielectric constant, or both. The result of the fit is shown in Fig. 3(a) as a red solid line. We obtain good agreement with the experiment with an effective static dielectric constant of $\kappa_0 \approx 13$ and a Fermi energy of $E_F/k_B \approx 100$ K, which is consistent with the experimental dielectric function ε_1 (Fig. 2) and the fit to the Drude-Boltzmann weight [Eq. (3)], respectively. The Landau pole takes an anomalously small value of $\Lambda_L \approx 600$ K, giving rise to strong superlinear scaling. This could be taken as an indirect sign that the material hosts pairs of Weyl cones in close proximity, consistent with the picture of a Weyl semimetal state with broken time-reversal symmetry. For comparison, we also include a fit of the intrinsic finite-temperature plasmon in Fig. 3(a) (dash-dotted magenta line). As before, the intrinsic result captures the high-temperature behavior where the Weyl state is most expected and the saturation at low temperature can be attributed to finite doping. Intuitively, one could expect a characteristic step in $\sigma_1(\omega)$ at $2E_F \approx 140$ cm^{-1}, but it should be smeared out by the large scattering rate and cannot be seen clearly in Fig. 2(b).

Linear (or quasilinear) dependence of the low frequency optical conductivity—a signature of a Dirac semimetallic state—has also been recently reported in several other 3D materials: HgCdTe [35], quasicrystals [36], and ZrTe$_5$ [37]. A notable result of our work compared to previous studies is the excellent agreement of the experimental and theoretical temperature dependent Drude spectral weight providing strong evidence of a Weyl state with finite doping. However, the independence of the Drude parameters on temperature in the paramagnetic state above T_N is surprising and merits further study.

In summary, the optical response of a Eu$_2$Ir$_2$O$_7$ single crystal reveals a semimetallic electronic structure with approximately linear frequency dependence of the optical conductivity down to 3 meV at low temperature. Below T_N, the Drude spectral weight diminishes consistent with the reduced thermal excitations of a Weyl semimetal. This means that the long-thought "metal-insulator" transition in pyrochlore iridates may actually be a metal-semimetal transition, at least in the case of Eu$_2$Ir$_2$O$_7$. These two data sets can be modeled assuming a Weyl state, as 24 Weyl cones with an average Fermi velocity $\bar{v}_F = 4 \times 10^7$ cm/s. The theoretical analyses of our optical data point toward signatures of the ultraviolet renormalization expected for an interacting Dirac liquid manifesting in the superlinear temperature dependence of the Drude weight.

[1] D. Pesin and L. Balents, Nat. Phys. **6**, 376 (2010).
[2] X.-L. Qi and S.-C. Zhang, Rev. Mod. Phys. **83**, 1057 (2011).
[3] M. Z. Hasan and C. L. Kane, Rev. Mod. Phys. **82**, 3045 (2010).
[4] M. Z. Hasan and J. E. Moore, Annu. Rev. Condens. Matter Phys. **2**, 55 (2011).
[5] S.-Y. Xu, C. Liu, S. K. Kushwaha, T.-R. Chang, J. W. Krizan, R. Sankar, C. M. Polley, J. Adell, T. Balasubramanian, K. Miyamoto, N. Alidoust, G. Bian, M. Neupane, I. Belopolski, H.-T. Jeng, C.-Y. Huang, W.-F. Tsai, H. Lin, F. C. Chou, T. Okuda, A. Bansil, R. J. Cava, and M. Z. Hasan, arXiv:1312.7624.
[6] Z. K. Liu, B. Zhou, Y. Zhang, Z. J. Wang, H. M. Weng, D. Prabhakaran, S.-K. Mo, Z. X. Shen, Z. Fang, X. Dai, Z. Hussain, and Y. L. Chen, Science **343**, 864 (2014).
[7] M. Neupane, S.-Y. Xu, R. Sankar, N. Alidoust, G. Bian, C. Liu, I. Belopolski, T.-R. Chang, H.-T. Jeng, H. Lin, A. Bansil, F. Chou, and M. Z. Hasan, Nat. Commun. **5**, 3786 (2014).
[8] Z. K. Liu, J. Jiang, B. Zhou, Z. J. Wang, Y. Zhang, H. M. Weng, D. Prabhakaran, S.-K. Mo, H. Peng, P. Dudin *et al.*, Nat. Mater. **13**, 677 (2014).
[9] S. Borisenko, Q. Gibson, D. Evtushinsky, V. Zabolotnyy, B. Büchner, and R. J. Cava, Phys. Rev. Lett. **113**, 027603 (2014).
[10] S.-Y. Xu, C. Liu, I. Belopolski, S. K. Kushwaha, R. Sankar, J. W. Krizan, T.-R. Chang, C. M. Polley, J. Adell, T. Balasubramanian *et al.*, Phys. Rev. B **92**, 075115 (2015).
[11] B. Q. Lv, N. Xu, H. M. Weng, J. Z. Ma, P. Richard, X. C. Huang, L. X. Zhao, G. F. Chen, C. E. Matt, F. Bisti *et al.*, Nat. Phys. **11**, 724 (2015).
[12] S.-Y. Xu, I. Belopolski, N. Alidoust, M. Neupane, G. Bian, C. Zhang, R. Sankar, G. Chang, Z. Yuan, C.-C. Lee *et al.*, Science **349**, 613 (2015).
[13] S.-Y. Xu, N. Alidoust, I. Belopolski, Z. Yuan, G. Bian, T.-R. Chang, H. Zheng, V. N. Strocov, D. S. Sanchez, G. Chang *et al.*, Nat. Phys. **11**, 748 (2015).
[14] X. Wan, A. M. Turner, A. Vishwanath, and S. Y. Savrasov, Phys. Rev. B **83**, 205101 (2011).
[15] W. Witczak-Krempa, G. Chen, Y. B. Kim, and L. Balents, Annu. Rev. Condens. Matter Phys. **5**, 57 (2014).
[16] W. Witczak-Krempa, A. Go, and Y. Kim, Phys. Rev. B **87**, 155101 (2013).
[17] F. Ishii, Y. P. Mizuta, T. Kato, T. Ozaki, H. Weng, and S. Onoda, J. Phys. Soc. Jpn. **84**, 073703 (2015).
[18] H. Shinaoka, S. Hoshino, M. Troyer, and P. Werner, Phys. Rev. Lett. **115**, 156401 (2015).
[19] H. Zhang, K. Haule, and D. Vanderbilt, arXiv:1505.01203.
[20] K. Matsuhira, M. Wakeshima, Y. Hinatsu, and S. Takagi, J. Phys. Soc. Jpn. **80**, 094701 (2011).
[21] S. Nakatsuji, Y. Machida, Y. Maeno, T. Tayama, T. Sakakibara, J. v. Duijn, L. Balicas, J. N. Millican, R. T. Macaluso, and J. Y. Chan, Phys. Rev. Lett. **96**, 087204 (2006).
[22] Y. Machida, S. Nakatsuji, S. Onoda, T. Tayama, and T. Sakakibara, Nature (London) **463**, 210 (2010).
[23] H. Takatsu, K. Watanabe, K. Goto, and H. Kadowaki, Phys. Rev. B **90**, 235110 (2014).
[24] K. Ueda, J. Fujioka, Y. Takahashi, T. Suzuki, S. Ishiwata, Y. Taguchi, and Y. Tokura, Phys. Rev. Lett. **109**, 136402 (2012).
[25] Y. S. Lee, S. J. Moon, Scott C. Riggs, M. C. Shapiro, I. R. Fisher, Bradford W. Fulfer, Julia Y. Chan, A. F. Kemper, and D. N. Basov, Phys. Rev. B **87**, 195143 (2013).
[26] J. J. Ishikawa, E. C. T. O'Farrell, and S. Nakatsuji, Phys. Rev. B **85**, 245109 (2012).
[27] See Supplemental Material at http://link.aps.org/supplemental/10.1103/PhysRevB.92.241108 for more details on fitting procedures.
[28] A. B. Kuzmenko, Rev. Sci. Instrum. **76**, 083108 (2005).
[29] J. F. McCaffrey, N. T. McDevitt, and C. M. Phillippi, J. Opt. Soc. Am. **61**, 209 (1971).
[30] L. Hozoi, H. Gretarsson, J. P. Clancy, B.-G. Jeon, B. Lee, K. H. Kim, V. Yushankhai, P. Fulde, D. Casa, T. Gog *et al.*, Phys. Rev. B **89**, 115111 (2014).
[31] R. E. Throckmorton, J. Hofmann, E. Barnes, and S. Das Sarma, Phys. Rev. B **92**, 115101 (2015).
[32] S. Das Sarma and E. H. Hwang, Phys. Rev. B **91**, 195104 (2015).
[33] J. Hofmann and S. Das Sarma, Phys. Rev. B **91**, 241108 (2015).
[34] D. E. Kharzeev, R. D. Pisarski, and H.-U. Yee, Phys. Rev. Lett. **115**, 236402 (2015).
[35] M. Orlita, D. M. Basko, M. S. Zholudev, F. Teppe, W. Knap, V. I. Gavrilenko, N. N. Mikhailov, S. A. Dvoretskii, P. Neugebauer, C. Faugeras *et al.*, Nat. Phys. **10**, 233 (2014).
[36] T. Timusk, J. P. Carbotte, C. C. Homes, D. N. Basov, and S. G. Sharapov, Phys. Rev. B **87**, 235121 (2013).
[37] R. Y. Chen, S. J. Zhang, J. A. Schneeloch, C. Zhang, Q. Li, G. D. Gu, and N. L. Wang, Phys. Rev. B **92**, 075107 (2015).